Parameter Optimization of a Discrete Scattering Model by Integration of Global Sensitivity Analysis Using SMAP Active and Passive Observations

Xiaojing Bai, Jiangyuan Zeng, *Member, IEEE*, Kun-Shan Chen, *Fellow, IEEE*, Zhen Li, *Member, IEEE*, Yijian Zeng, Jun Wen, Xin Wang, Xiaohua Dong, and Zhongbo Su

***Abstract*— Active and passive microwave signatures respond differently to the land surface and provide complementary information on the characteristics of the observed scenes. The objective of this paper is to explore the synergy of active radar and passive radiometer observations at the same spatial scale to constrain a discrete radiative transfer model, the Tor Vergata (TVG) model, to gain insights into the microwave scattering and emission mechanisms over grasslands. The TVG model can simultaneously simulate the backscattering coefficient and emissivity with a set of input parameters. To calibrate this model, in situ soil moisture and temperature data collected from the Maqu area in the northeastern region of the Tibetan Plateau, interpolated leaf area index (LAI) data from the Moderate Resolution Imaging Spectroradiometer LAI eight-day products, and concurrent and coincident Soil Moisture Active Passive (SMAP) radar and radiometer observations are used. Because this model needs numerous input parameters to be driven, the extended Fourier amplitude sensitivity test is first applied to conduct global sensitivity analysis (GSA) to select the sensitive and insensitive parameters. Only the most sensitive parameters are defined as free variables, to separately calibrate the active-only model (TVG-A), the passive-only model (TVG-P), and the active and passive combined model (TVG-AP). The accuracy of the calibrated models is evaluated by comparing the SMAP observations and the model simulations. The results show that TVG-AP can well reproduce the backscattering coefficient and brightness temperature, with correlation coefficients of 0.87, 0.89, 0.78, and 0.43 and root-mean-square errors of 0.49 dB, 0.52 dB, 7.20 K, and 10.47 K for σ^o_{HH}, σ^o_{VV}, T_{BH}, and T_{BV}, respectively. In contrast, TVG-A and TVG-P can only accurately model the backscattering coefficient and brightness temperature, respectively. Without any modifications of the calibrated parameters, the error metrics computed from the validation data are slightly worse than those of the calibration data. These results demonstrate the feasibility of the synergistic use of SMAP active radar and passive radiometer observations under the unified framework of a physical model. In addition, the results demonstrate the necessity and effectiveness of applying GSA in model optimization. It is expected that these findings can contribute to the development of model-based soil moisture retrieval methods using active and passive microwave remote sensing data.**

***Index Terms*— Active and passive microwave, calibration and validation, global sensitivity analysis (GSA), Soil Moisture Active Passive (SMAP), soil moisture, Tor Vergata (TVG) model.**

Manuscript received April 7, 2018; revised June 13, 2018 and July 24, 2018; accepted July 31, 2018. This work was supported in part by the National Key Research and Development Program of China under Grant 2018YFA0605403, in part by the National Natural Science Foundation of China under Grant 41601371 and Grant 41531175, and in part by the startup foundation for introducing talent of NUIST under Grant 2017r087. The work of J. Zeng was supported by the Youth Innovation Promotion Association CAS under Grant 2018082. *(Corresponding author: Jiangyuan Zeng.)*

X. Bai is with the School of Hydrology and Water Resources, Nanjing University of Information Science and Technology, Nanjing 210044, China.

J. Zeng and K.-S. Chen are with the State Key Laboratory of Remote Sensing Science, Jointly Supported by the Institute of Remote Sensing and Digital Earth, Chinese Academy of Sciences and Beijing Normal University, Beijing 100101, China (e-mail: zengjy@radi.ac.cn).

Z. Li is with the Airborne Remote Sensing Center, Institute of Remote Sensing and Digital Earth, Chinese Academy of Sciences, Beijing 100094, China.

Y. Zeng and Z. Su are with the Faculty of Geo-Information Science and Earth Observation, University of Twente, 7500 AE Enschede, The Netherlands.

J. Wen is with the College of Atmospheric Sciences, Plateau Atmosphere and Environment Key Laboratory of Sichuan Province, Chengdu University of Information Technology, Chengdu 610225, China.

X. Wang is with the Key Laboratory of Land Surface Process and Climate Change in Cold and Arid Regions, Northwest Institute of Eco-Environment and Resources, Chinese Academy of Sciences, Lanzhou 730000, China.

X. Dong is with the College of Hydraulic and Environmental Engineering, China Three Gorges University, Yichang 443002, China.

Color versions of one or more of the figures in this paper are available online at http://ieeexplore.ieee.org.

Digital Object Identifier 10.1109/TGRS.2018.2864689

I. Introduction

SURFACE soil moisture is an important state variable for regulating regional and global water cycle, energy balance, and climate change on the earth's surface [1]–[3]. A good knowledge of the spatial and temporal distributions of soil moisture can help in understanding the role of hydrological processes in the climate system [1], [2]. Despite the particular usefulness of soil moisture, quantitative measurements of soil moisture at different spatial scales (especially at large scales) by using traditional hydrometeorological stations remain very difficult, due to the considerable heterogeneity of the land surface [4]. Microwave remote sensing, both active and passive, provides an effective technique to characterize the distribution of soil moisture at the regional and global scales [3], [4]. This technique has been demonstrated to be the best way to infer soil moisture spatially and temporally at large scales, owing to its high sensitivity to soil permittivity and its capability for 24-h all-weather coverage [2]–[6]. Active microwave sensors, especially synthetic aperture radar, can provide soil

moisture data at a fine spatial resolution [2], [7], [8]. However, radar backscatter is highly susceptible to scattering and attenuation effects from vegetation and surface roughness [4]. In contrast, passive microwave sensors, e.g., radiometers, are able to map soil moisture with higher temporal resolution and with reduced sensitivity to vegetation and surface roughness compared with that of active sensors [9]. The main drawback of passive radiometry is that its spatial resolution is often very coarse (i.e., dozens of kilometers), which limits its usage in some practical applications, such as agricultural productivity estimation at a local scale [4]. Since radar and radiometers can offer complementary information on soil moisture, a joint use of both instruments provides an opportunity to improve the accuracy of soil moisture retrieval by leveraging the complementary strengths of active and passive measurements [10], [11].

The first satellite equipped with both active and passive instruments was the Aquarius/SAC-D mission, a joint program between the National Aeronautics and Space Administration (NASA) and Argentina's Space Agency (Comisión Nacional de Actividades Espaciales), launched in 2011 [12]. The satellite consists of a fully polarimetric L-band (1.26 GHz) scatterometer and three dual-polarized L-band (1.413 GHz) radiometers [12]. This mission was originally designed for measuring sea surface salinity but has also been used for monitoring soil moisture [13]. The dedicated soil moisture observation system, which integrates radar and radiometry in a single satellite, is NASA's Soil Moisture Active Passive (SMAP) mission, launched on January 31, 2015 [10]. The device carries an L-band radar instrument (1.26 GHz) and an L-band radiometer (1.41 GHz), which are colocated at a constant incidence angle of 40°, and has shown good performance in terms of soil moisture estimation [14], [15]. Though the SMAP radar ceased working on July 7, 2015, the active–passive synergistic algorithm can be used by implementing alternative active measurements, e.g., the ongoing Sentinel-1 C-band data [16], [17] and the upcoming Water Cycle Observation Mission data [18]. Fortunately, the science data from SMAP released to the public now include over two months of coincident spaceborne active radar and passive radiometer measurements with an unprecedented spatial resolution, which provides us with a unique opportunity and motivation to fully explore the complementarity of active and passive observations [19].

Several methodologies have been developed to take advantage of the respective strengths of radar and radiometer measurements for surface modeling and soil moisture retrieval. The first scheme uses fine scale radar observations to downscale coarse passive soil moisture products (see [20]). The second scheme utilizes fine scale radar observations to enhance the spatial resolution of radiometer data, which are then employed to retrieve fine scale soil moisture. For example, the SMAP active–passive baseline algorithm is used to disaggregate the coarse radiometer brightness temperature using concurrent fine scale radar acquisitions, and soil moisture is retrieved from the downscaled brightness temperature [21], [22]. The third scheme directly merges the two single-source soil moisture products retrieved from the active and passive observations to obtain a complete and consistent global soil moisture data record. For example, the European Space Agency climate change initiative soil moisture product is blended from several active and passive soil moisture products to produce a long-term and unified soil moisture data set [23], which introduces the advantages of spatial coverage and temporal extension [24]. The fourth scheme uses machine-learning methods, e.g., artificial neural networks [25]–[27] and the Bayesian algorithm [28], to retrieve soil moisture from the combination of active and passive microwave data. The aforementioned schemes are generally data-driven-based approaches that ignore a physical interpretation of land surface scattering and emission mechanisms. The fifth scheme combines complementary information from active and passive microwave remote sensing by using physics-based radar and radiometer forward models, which are capable of simultaneously simulating the backscattering coefficient and emissivity. The radar backscatter forward model and radiometer brightness temperature forward model independently predict the backscatter and emissivity, which are used to build a joint active and passive cost function for soil moisture retrieval [11], [19]. The discrete scattering model, which is a unified model, is also constrained by the combined use of active and passive microwave observations and can be used for surface modeling [29] and soil moisture retrieval [30].

In this paper, we focus on the use of a unified approach, which is a physically based active and passive forward model, to account for the scattering and emission processes simultaneously, for which there have been limited studies conducted. Dente *et al.* [29] combined Advanced Scatterometer (ASCAT) data and AMSR-E data to constrain a discrete scattering model for simulating both backscatter and emission. Wang *et al.* [30] adopted concurrent active and passive Aquarius observations to estimate soil moisture using the same discrete electromagnetic model. These two studies demonstrated the feasibility of using unified scattering and emission models for the synergy of active and passive microwave observations. However, the ASCAT and AMSR-E data used in [29] were acquired at different local times and incidence angles, which inevitably introduces in representative errors. Moreover, the spatial resolution of the Aquarius observations used in [30] is very coarse (∼100 km), which results in higher land surface heterogeneity within the satellite's observation footprint, and thus introduces more uncertainties [31], [32]. In addition, it is well known that discrete scattering models often need numerous input parameters, which are very difficult to estimate. For this reason, it is necessary to select the most sensitive parameters for model optimization. Dente *et al.* [29] and Wang *et al.* [30] have adopted local sensitivity analysis (LSA) to distinguish the sensitive and insensitive parameters. It is well known that many parameters (e.g., soil moisture and vegetation) usually vary simultaneously in the natural world. However, LSA can only explain the sensitivity of each parameter when fixing all of the remaining parameters at their nominal values and cannot quantify the effects of interactions among the parameters [33]. In addition, the credibility of LSA in nonlinear models is questionable [34]. Discrete scattering models are often nonlinear and nonmonotonic, which limits

the application of LSA. Compared with LSA, global sensitivity analysis (GSA) can analyze parameters' sensitivities over the entire parameter space [35]. Moreover, GSA can consider the comprehensive effects of the parameters on the model outputs. Due to these advantages, GSA can be applied to identify the sensitive and insensitive parameters of discrete scattering models more efficiently and reliably than LSA can.

In this context, we investigate and evaluate, for the first time, the effectiveness and necessity of applying GSA to optimize a discrete scattering model, the Tor Vergata (TVG) model [36], [37] using active and passive SMAP observations. TVG is a discrete radiative transfer model that is capable of simultaneously simulating the backscattering coefficient and emissivity. This model has widely been applied to surface modeling [29], soil moisture retrieval [30], vegetation moisture monitoring [38], and freeze-thaw process detection [39]. TVG is driven by a set of input parameters including sensor configuration and soil and vegetation parameters. A GSA method, i.e., the extended Fourier amplitude sensitivity test (EFAST) algorithm [40], is adopted to rank the sensitivity of the input parameters for this model. Only the most sensitive parameters are defined as free variables to be calibrated. Model calibration and validation are implemented by comparing the model simulations and SMAP observations in the Tibetan Plateau. *In situ* measurements collected from the Maqu network, SMAP observations, and Moderate Resolution Imaging Spectroradiometer (MODIS) products are together used for model calibration and validation. Nearly 60% of the data from SMAP's full sensor suite are used for model calibration, and the remaining data are used for validation.

This paper is organized as follows. Section II introduces the study area, *in situ* measurements, SMAP data, and MODIS data. Section III describes the TVG model, the GSA method, and the method used for model calibration and validation. The results are presented in Sections IV from three perspectives: GSA, model calibration, and model validation. Discussions are presented in Section V in terms of four considerations: selection of sensitive parameters, contribution of leaf area index (LAI), uncertainties in model calibration, and considerations in the use of GSA. Conclusions of this paper are summarized in Section VI.

II. Materials

A. Study Area

In this paper, *in situ* soil moisture and temperature measurements are collected from the Maqu soil temperature and moisture network (33° 30′−34° 15′ N, 101° 38′−102° 45′ E) [1], which is located at the northeastern edge of the Tibetan Plateau, shown in Fig. 1. This network was established in July 2008, and to date, there are 20 monitoring stations distributed throughout the southern part of Maqu County, with an average elevation of approximately 3470 m. The location of the Maqu soil temperature and moisture network and distribution of the corresponding stations are displayed in Fig. 1. The soil moisture and temperature are continuously measured at different soil depths (5, 10, 20, 40, and 80 cm) in 15-min intervals by means of 5TM ECH$_2$O probes (Decagon Devices, Inc., Pullman, WA, USA). The dominant land cover is

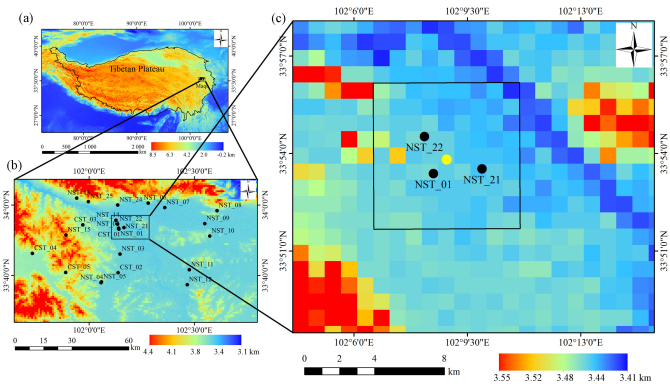

Fig. 1. Geographical locations of (a) Maqu network, (b) monitoring stations on the Tibetan Plateau, and (c) study area used in this paper, with the background indicating the digital elevation model from the shuttle radar topography mission with a spatial resolution of 1 km.

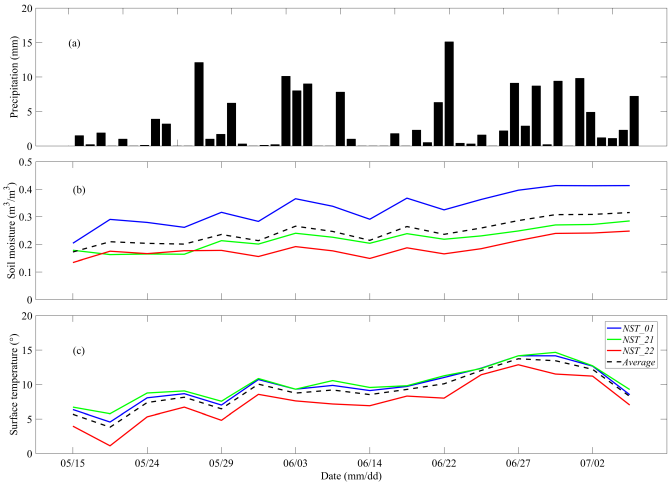

Fig. 2. Time series of (a) daily precipitation, (b) *in situ* soil moisture, and (c) surface temperature in the study area from April 2015 to July 2015.

seasonal grassland. The soil is characterized by silt loam soils, and its texture parameters were determined from undisturbed soil samples collected during station installation. More details about the Maqu soil temperature and moisture network can be found in [1] and [41].

To match the spatial resolution of SMAP observations, a specific region with 9 km × 9 km is selected as the study area [Fig. 1(c)], with the yellow circle indicating the geographical center. There are three stations, named NST_01, NST_21, and NST_22, in the selected SMAP grid cell, and the average *in situ* soil moisture and temperature at a depth of 5 cm at these three stations are considered as the soil conditions of this grid [4], [14]. The *in situ* soil moisture and temperature, averaged using data from 06:00 AM and 06:15 AM. Beijing standard time at the selected stations, are shown in Fig. 2; the selected times correspond to the acquisition times (descending pass) of SMAP. The reason for selecting this time period is to minimize the difference between vegetation and soil temperature, since in the morning (e.g., 6:00 AM), the air, vegetation, and near-surface soil are in thermal equilibrium [14], [15], [42]. Daily precipitation

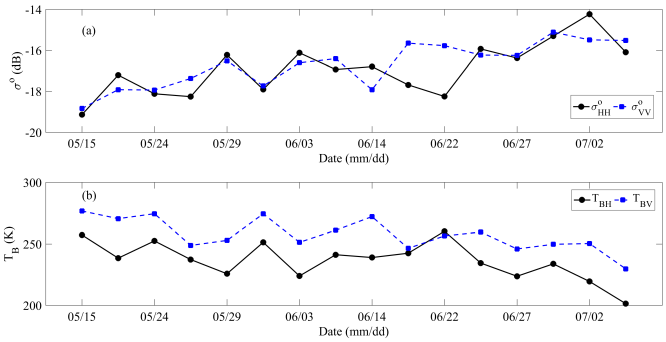

Fig. 3. Temporal evolution of (a) SMAP backscattering coefficient and (b) brightness temperature in the study area from May 2015 to July 2015.

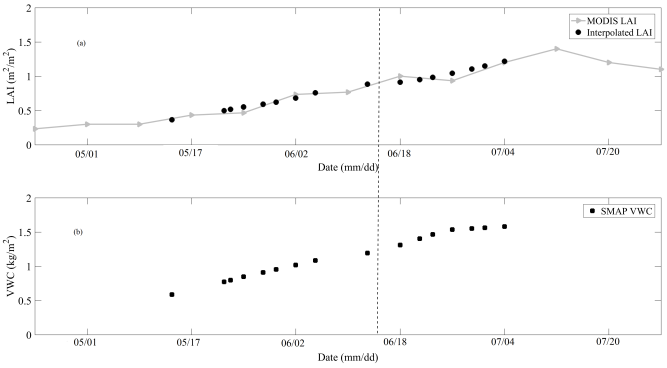

Fig. 4. Time evolution of (a) MODIS LAI and interpolated LAI data and (b) SMAP VWC in the study area from May 2015 to July 2015.

data from April 2015 to July 2015, which can be downloaded from the China Meteorological Data Sharing Service System of the China Meteorological Administration (http://data.cma.gov.cn/), are used. From Fig. 2, it can be seen that the pattern of soil moisture is consistent with the trend of precipitation and that the soil temperature continues to rise during the selected period.

B. SMAP Data

In this paper, the SMAP Level-3 radar/radiometer global daily EASE-Grid2 soil moisture product (version 3, SPL3SMAP) with a grid resolution of 9 km is used. The temporal coverage of this product ranges from April 13, 2015 to July 7, 2015. The SPL3SMAP product includes brightness temperature, backscattering coefficients, soil moisture, and other auxiliary data. The SMAP data were downloaded from the National Snow and Ice Data Center (https://nsidc.org/data/SMAP/SMAP-data.html). All available backscattering coefficient and brightness temperature data in the study area are shown in Fig. 3.

The SMAP active–passive soil moisture product is retrieved from L-band radar and radiometer observations using a downscaling approach [22]. The key to this approach is to disaggregate the radiometer brightness temperature from 36 to 9 km by using concurrent radar backscatter at a fine resolution of 3 km. To effectively constrain the model variables, active σ^o_{HH} and σ^o_{VV} data combined with passive T_{BH} and T_{BV} data are used in this paper.

The reason for selecting the SMAP active–passive disaggregated brightness temperature instead of the SMAP enhanced brightness temperature in our study is mainly due to the heterogeneity of our study area. It is well known that the geographical environment and climate conditions of Tibetan Plateau are quite different compared with those of other places in the world. In previous studies, it has been found that the performance of current passive remotely sensed soil moisture products is still not satisfactory in the Tibetan Plateau [24], which may be due to the heterogeneity (e.g., surface roughness) of the area. As stated above, the SMAP disaggregated brightness temperature is downscaled by using concurrent high-resolution radar data. In particular, HV-polarized backscatter is used to account for the heterogeneity of the 9 km grid within the 36 km grid. That is, the disaggregated 9 km brightness temperature data are considered to reflect the heterogeneity of the observed surface. In contrast, the enhanced brightness temperature is interpolated from the original 36 km brightness temperature data, which may cause a loss of heterogeneity in the observed surface. Therefore, the active–passive disaggregated brightness temperature is used instead of the enhanced brightness temperature in this paper.

C. MODIS Data

LAI data are used as model input parameters to characterize the vegetation conditions. The Terra MODIS LAI 8-day products with a spatial resolution of 1 km, which are released by NASA Goddard Space Flight Center Level 1 and Atmosphere Archive and Distribution System (http://ladsweb.nascom.nasa.gov/data/search.html), are used. The preprocessing for the MODIS LAI products includes reprojection, resampling, smoothing, and interpolation. The spatial resolution of the original SIN Grid data is resampled from 1 to 9 km to be consistent with the observation scales of SMAP. The third Savitzky–Golay filter is used to smooth the MODIS LAI data to suppress the effect of cloud cover [43]. To compute the LAI values on the acquisition dates of SMAP observations, the smoothed LAI data are interpolated with the cubic spline interpolation technique. Fig. 4 presents the original MODIS LAI data, interpolated LAI data, and vegetation water content (VWC) extracted from the SMAP Level-3 radar/radiometer soil moisture product. The calibration and validation data are distinguished by a dashed line.

III. Methodology

In this paper, the active and passive versions of the TVG model are applied to simulate the backscattering coefficient and emissivity by integrating the *in situ* measurements, SMAP observations, and interpolated LAI data from MODIS LAI products in the Maqu region. The GSA method is applied to rank the input parameters and select the most sensitive parameters for model calibration. The implementation of the GSA, model calibration, and model validation can be found in Fig. 5, and detailed descriptions are introduced in Sections III-B and III-C.

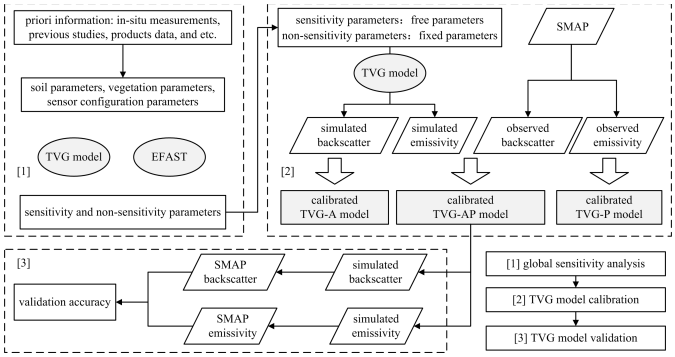

Fig. 5. Implementation of the GSA, model calibration, and model validation.

A. TVG Model

To simulate the backscattering coefficient and emissivity over the grasslands, a discrete radiative transfer model developed at the University of Rome TVG is used [36], [37], which will be simply referred to as "the model." Like other discrete scattering models, this model simultaneously considers the contributions from soil and vegetation. In both active and passive versions of this model, the vegetation is modeled as an ensemble of discrete lossy scatterers, whose electromagnetic behaviors are simulated by simple geometrical shapes, e.g., cylinders and discs. The basic components that constitute vegetation include stems, leaves, and needles, and their scattering and absorption properties are dependent on the ratio between the element size and the wavelength. The stems and needles are all modeled as dielectric cylinders using the Rayleigh–Gans approximation [44] in the L-band or the infinite length approximation [45], depending on frequency and size. The geometric parameters needed to simulate the scattering and absorption of the cylindrical shapes include the radius, length (or height), and gravimetric moisture (fraction) of the cylinders, and the number of cylinders per unit of underlying area. The leaves are represented as circular discs, whose scatter matrices and extinction vector are computed using the Rayleigh–Gans approximation [44], [46] and physical optics approximation [47], depending on frequency. The geometric parameters required for the discs include the disc radius, disc thickness, plant moisture content (fraction), and disc angular distribution. The disc angular distribution is generally assumed to be random. The soil surface is described as a homogeneous half-space with a rough interface, whose electromagnetic behavior is approximated by the integral equation model (IEM) [48]. The surface soil parameters needed to implement the IEM are the volumetric soil moisture, soil temperature, soil texture, root-mean-square (rms) height, correlation length, and autocorrelation function.

When the individual scattering and attenuation properties of vegetation components and soil are determined, the matrix doubling method is used to compute the scattering matrix of the whole soil-vegetation system [49]. The backscattering coefficient and the emissivity are finally computed at selected frequencies and incidence angles, respectively. To compute the vegetation permittivity and soil permittivity, the Mätzler [50] vegetation mixing model and Dobson [51] dielectric mixing model are used, respectively. Details about the active and passive versions of the model can be found in [36] and [37]. This model has achieved a good performance for agricultural fields within the L-band and at higher frequencies [52]–[54]. Recently, this model has been adopted to simulate the backscattering coefficient and emissivity over a grassland region by considering the component of grassland litter, which consisted of dry grass leaves from the previous year [29]. Dente *et al.* [29] and Wang *et al.* [30] found that the contribution of litter is very important for simulating C-band and L-band satellite observations in the Maqu region. The contribution of litter is modeled as a mixture of air and dielectric material overlaying the soil [55]. The scattering matrices for the litter are modeled by the litter thickness, litter biomass, and litter gravimetric moisture content. The soil and litter are assumed to have an equivalent permittivity, which is included in the IEM model.

The backscattering coefficient is computed from the bistatic scattering coefficient in the opposite direction of incidence only, while the computation of emissivity is based on the energy conservation law by integrating all bistatic scattering coefficients across the hemisphere that yields the reflectivity [36], [37]. The brightness temperature is computed by multiplying the modeled emissivity (one minus reflectivity) by the effective temperature, which is approximated by the *in situ* topsoil temperature (i.e., 5 cm). It should be noted that the direct use of topsoil temperature as the effective temperature is not always valid [56], [57]. However, at the Maqu site, Lv *et al.* [58] showed that the 5 cm soil temperature can be approximately representative of the effective temperature.

In this paper, three components, including the soil surface, leaves, and litter, are considered to model the scattering processes of grasslands in Maqu. Although the contribution of vegetation is small within the L-band at this site, we use the complete model, including soil and vegetation contributions. The simulation of backscattering and emissivity is conducted under the SMAP configuration. The frequencies for the active and passive versions of the model are set as 1.26 and 1.41 GHz, respectively, and the incidence angle is set as 40° for both. The distribution and ranges of soil moisture and LAI are defined according to the *in situ* soil moisture and interpolated LAI data. The exponential correlation function is found to be capable of characterizing natural land cover within the L-band [59], [60], and thus is adopted in our study. The default values for other input parameters are obtained from [29], which was performed in the same study area. The parameter ranges are proportionally amplified from a $\pm 50\%$ perturbation based on the default values. Previous studies [33], [61] have found that the distribution of parameters had a very small impact on the GSA results, and a uniform distribution is commonly assumed regarding the input factors. Since there is no prior knowledge for the input parameters, most of them are assumed to be uniformly distributed. The plant moisture content stands for the ratio between the difference in fresh and dry biomass and the fresh biomass. The specific distribution and ranges for the input parameters required by the model and adopted in the sensitivity analysis are given in Table I.

TABLE I
DISTRIBUTIONS AND RANGES FOR THE INPUT PARAMETERS OF THE MODEL ADOPTED IN GSA

Input	Definition	Label	Distribution	Default	Range
Sensor	frequency (GHz)	f	-	1.26 and 1.41	
	incidence angle (°)	θ	-	40	
Soil surface	soil moisture (m^3/m^3)	sm	uniform	0.24	0.17-0.32
	RMS height (cm)	sig	uniform	0.9	0.2-4.0
	correlation length (cm)	l	uniform	9.0	6.0-40.0
	autocorrelation function	ACF	-	exponential	
Canopy	LAI (cm^2/cm^2)	lai	normal	0.80 (0.26)	0.1-1.9
Leaves	disc radius (cm)	add	uniform	1.4	0.7-2.1
	disc thickness (cm)	ldd	uniform	0.02	0.01-0.03
	plant moisture content	$amoidd$	uniform	0.8	0.4-1.0
	disc angular distribution	-	-	random	
Litter	litter moisture content (cm)	$gmoist$	uniform	0.48	0.24-0.72
	litter biomass (g/cm^2)	$biomass$	uniform	0.07	0.035-0.105
	litter thickness (cm)	$thickness$	uniform	0.6	0.3-0.9

B. GSA Method

It is known that the backscatter and emissivity are both influenced by a number of variables. It is very difficult, if not impossible, to calibrate all the input parameters of the model. Thus, the relative contributions of each input parameter to the backscatter and emissivity have to be quantified, which helps discriminate between the sensitive and insensitive parameters for calibrating the model. The most sensitive parameters are selected as free variables constrained within the parameter ranges, and the insensitive parameters are set as default values based on previous experience.

In this paper, a GSA method, i.e., the EFAST algorithm [40], is adopted to rank the input parameters and select the most sensitive parameters for the active and passive models. EFAST is a variance-based global and quantitative sensitivity analysis method, which combines the advantages of a high efficiency of sampling, from the Fourier amplitude sensitivity test, and of considering the individual and interaction effects, from the Sobol's method. Compared with LSA methods, EFAST is capable of analyzing complex nonlinear and nonmonotonic models and is currently recognized as one of the most elegant methods for sensitivity analysis.

Implementing the EFAST algorithm primarily includes two steps. The first procedure is called resampling, which is performed via a transformation function.

For a given model simplified as

$$y = f(x), \quad x = (x_1, x_2, \ldots, x_n) \tag{1}$$

where x_1 to x_n represent the n input parameters, the multidimensional input parameter space is first converted into a 1-D space through the Fourier transformation functions called searching curves

$$x_i(s) = \frac{1}{2} + \frac{1}{\pi} \arcsin[\sin(w_i s + \varphi_i)] \tag{2}$$

where $i = 1, 2, \ldots, n$, ϕ_i is the random phase shift within $[0,2\pi)$, w_i is the Fourier frequency, and s stands for the sample order from 1 to the total number of samples. The key for this procedure is to select the critical parameters. Saltelli *et al.* [40] have given an explicit computation formula

$$C = nN_s = nN_r(2\mathrm{M}w_{\max} + 1) \tag{3}$$

where C is the expected random number, n stands for the number of parameters ($n = 10$), N_s is the sample size, N_r is the number of curves explored, M is the interference factor ($M = 4$), and $\omega_{\max}$ is the largest sampling frequency. To reasonably obtain this number, some constraints are necessary

$$w_{\max} \geq 8; \quad \frac{w_{\max}}{N_r} \in [16, 64]. \tag{4}$$

From (3) and (4), it can be seen that the number of random samples depends on the values of $\omega_{\max}$ and N_r, which highly affect the convergence of the sensitivity indices (SIs). To compromise between computation and convergence, $\omega_{\max}$ and N_r are set as 128 and 4, respectively. Once these two parameters are determined, N_s is 4100 and the number of numerical experiments C is 41 000. The distributions and ranges for the input parameters in Table I are used to conduct the GSA of the TVG model. The second procedure is to compute the SIs for each input parameter. The SIs mainly include the main SI (MSI) and total SI (TSI), which are computed via the following procedures.

With the random input parameters, including the model $f(x)$, the model outputs can be transformed in the model's Fourier series expansion

$$y = f(s) = \sum_{j=-\infty}^{+\infty} \{\cos(js) + B_j \sin(js)\} \tag{5}$$

where A_j and B_j represent two Fourier coefficients, expressed as

$$A_j = \frac{1}{2\pi} \int_{-\pi}^{\pi} f(s) \cos(js) ds \tag{6a}$$

$$B_j = \frac{1}{2\pi} \int_{-\pi}^{\pi} f(s) \sin(js) ds. \tag{6b}$$

The total variance D of the model outputs is obtained as

$$D = \frac{1}{2\pi} \int_{-\pi}^{\pi} f^2(s) ds - \left[\frac{1}{2\pi} \int_{-\pi}^{\pi} f(s) ds\right]^2 \approx 2 \sum_{j=1}^{+\infty} \left(A_j^2 + B_j^2\right). \tag{7}$$

The estimated conditional variance D_i of the individual parameters is calculated as

$$D_i = 2 \sum_{j=1}^{+\infty} \left(A_{jw_i}^2 + B_{jw_i}^2\right). \tag{8}$$

Finally, MSI and TSI are defined as

$$\mathrm{MSI} = \frac{D_i}{D} \tag{9}$$

$$\mathrm{TSI} = 1 - \frac{D_{-i}}{D} \tag{10}$$

where $D_{(-i)}$ represents the estimated conditional variance except for the ith factor. For both MSI and TSI, higher values indicate greater sensitivity to the model outputs. The effective ranges for MSI and TSI are from 0 to 1. The difference between TSI and MSI (TSI–MSI) indicates the interactions between the parameters. A detailed description for computing MSI and TSI is provided in [40].

C. Model Calibration and Validation

Model calibration is an important procedure that helps to parameterize the unavailable input parameters. It should be mentioned that both the active and passive simulations have to be simultaneously applied to the satellite data. Thus, the following cost function S is constructed to make the model simulation approach the SMAP observations:

$$S = \frac{\mathrm{MAE}\left(\sigma^o_{\mathrm{HH}}\right)}{\Delta\sigma^o_{\mathrm{HH}}} + \frac{\mathrm{MAE}\left(\sigma^o_{\mathrm{VV}}\right)}{\Delta\sigma^o_{\mathrm{VV}}} + \frac{\mathrm{MAE}(T_{\mathrm{BH}})}{\Delta T_{\mathrm{BH}}} + \frac{\mathrm{MAE}(T_{\mathrm{BV}})}{\Delta T_{\mathrm{BV}}} \tag{11}$$

where MAE(•) stands for the mean absolute error between the model simulations and satellite observations and Δ indicates the standard deviation in satellite observations. The most challenging issue for selecting the cost function is how to balance the contributions of the active and passive parts. In [19], a regularization term is used to capture both the radar and radiometer contributions. In [30], four values are selected to obtain comparable weights for the backscatter and brightness temperature. The cost function used in our study, which is obtained from [29], is numerically normalized. The four parts in (11) are dimensionless. Therefore, it can be concluded that the active and passive parts contribute equally to obtaining the optimum parameters. A lookup table (LUT) method is applied to find a set of input parameters that can minimize the cost function. The LUT is established based on the free variables, which are selected based on the sensitivity analysis results. The number of combinations is computed as: 40 (rms height) $\times$18 (correlation length) $\times$5 (N) $\times$ 3 (litter biomass) $\times$3 (litter thickness) = 32 400. During the calibration process, the values for the cost function (11) are computed by executing the iteration of all the possible combinations. That is to say, we will find the minimum value of the cost function in all possible solutions (32 400). It means we search the optimal value among all possible combinations and we do not set any thresholds to determine the "optimized" cost function value.

In this paper, we select the first 60% of the data for model calibration, and the remaining data are used for model validation. Once the optimal sets of parameters are determined, they are used directly as input parameters for the model without any change. The simulated backscattering coefficient and brightness temperature are compared with the SMAP observations.

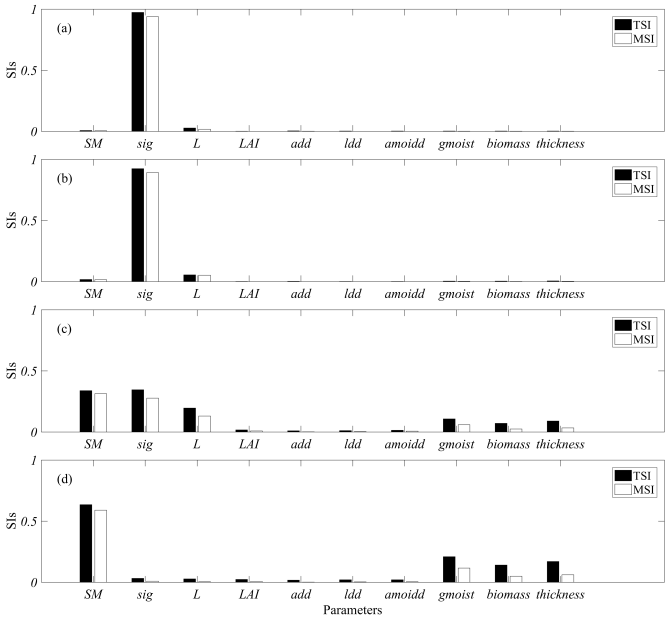

Fig. 6. Sensitivities of backscatter and emissivity to the input parameters in the TVG model. (a) σ^o_{HH}. (b) σ^o_{VV}. (c) T_{BH}. and (d) T_{BV}. TSI and MSI stand for the total sensitivity index and main sensitivity index, respectively.

Five error metrics, including the correlation coefficient (R), mean bias (Bias), MAE, root-mean-square error (RMSE), and unbiased RMSE, are adopted to evaluate the calibration and validation accuracy

$$R = \frac{\sum(d_{\mathrm{oi}} - \bar{d}_{\mathrm{oi}})(d_{\mathrm{si}} - \bar{d}_{\mathrm{si}})}{\sqrt{(d_{\mathrm{oi}} - \bar{d}_{\mathrm{oi}})^2}\sqrt{(d_{\mathrm{si}} - \bar{d}_{\mathrm{si}})^2}} \tag{12}$$

$$\mathrm{Bias} = \frac{1}{n}\left(\sum d_{\mathrm{oi}} - \sum d_{\mathrm{si}}\right) \tag{13}$$

$$\mathrm{MAE} = \frac{1}{n}\sum |d_{\mathrm{oi}} - d_{\mathrm{si}}| \tag{14}$$

$$\mathrm{RMSE} = \sqrt{\frac{1}{n}\sum (d_{\mathrm{oi}} - d_{\mathrm{si}})^2} \tag{15}$$

$$\mathrm{ubRMSE} = \sqrt{\mathrm{RMSE}^2 - \mathrm{Bias}^2} \tag{16}$$

where d_{oi} and d_{si} indicate the observed and simulated backscattering coefficients or brightness temperature, respectively, at a given time i, and $\bar{d}_{\mathrm{oi}}$ and $\bar{d}_{\mathrm{si}}$ are their average values, respectively.

IV. Results

A. Global Sensitivity Analysis

Since most of the input parameters for the model are unavailable, the EFAST method is applied to select the sensitive and insensitive parameters. In comparisons with SMAP observations, the sensitive parameters are used as free variables. The less sensitive parameters are set as constant values according to previous studies [29]. The input parameters and their ranges are listed in Table I, and the results of GSA are displayed in Fig. 6.

It is seen that for the active observations at VV and HH polarizations, the most sensitive parameter is the rms height. The second and third most influential parameters are

the correlation length and soil moisture, respectively. The remaining vegetation and litter parameters have little effect on the backscattering coefficient. For T_{BV}, in contrast, the soil moisture is the most sensitive parameter, and its TSI and MSI values are 0.63 and 0.59, respectively. The three litter parameters also have a high impact on emissivity, whereas the roughness and vegetation parameters play a secondary role in T_{BV}. Nevertheless, for T_{BH}, the three most sensitive parameters are rms height, soil moisture, and correlation length, which is similar to the results of σ^o_{HH} and σ^o_{VV}. This is in line with Zeng *et al.* [62], who found that T_{BV} had a much lower sensitivity to surface roughness than that of T_{BH}, especially at larger incidence angles. Compared with T_{BV}, T_{BH} is more sensitive to rms height and correlation length and less sensitive to the three litter parameters. According to the sensitivity analysis results, the parameterizations of the inputs used to calibrate the model are defined as follows.

1) *For Available Parameters:* The soil moisture and surface temperature are initialized by the *in situ* measurements. The interpolated LAI is used as input to characterize the growth of vegetation.
2) *For Unavailable But Sensitive Parameters:*For the active case, the rms height and correlation length have been found to have higher SI. For the passive case, the litter moisture content, litter biomass, and litter thickness have been found to have higher SI. For simultaneous simulation of the active and passive observations, these five parameters are defined as free variables, and their ranges are listed in Table I. The litter moisture content is defined as N times of the soil moisture, according to [29]. This is because in previous work, the litter moisture content has been assumed to have a linear relationship with the soil moisture [59]. In this paper, the values of N are set as 0.25, 0.5, 1, 1.5, and 2, respectively.
3) *For Unavailable and Insensitive Parameters:* The disc radius, disc thickness, and plant moisture content have been found to be insensitive to the backscatter and emissivity. In this paper, the values of these parameters are derived from [29] (see Table I).

B. Model Calibration

The model calibration is conducted by minimizing the cost function in (11) to determine the optimal set of input parameters. To highlight the advantage of the synergistic use of both active and passive microwave data, the active only, the passive only, and both the active and passive data are separately used to calibrate the model; these approaches are shortened as TVG-A, TVG-P, and TVG-AP, respectively. The optimal values of the five most sensitive parameters selected during the model calibration are listed in Table II, and the values of other input parameters are given in Table I. Figs. 7–9 display the temporal evolution of SMAP observations and simulated backscattering coefficients and brightness temperature obtained from TVG-A, TVG-P, and TVG-AP. The error metrics between the SMAP observations and model simulations are presented in Table III.

TABLE II

OPTIMAL VALUES OF THE FIVE MOST SENSITIVE PARAMETERS FOR THE TVG MODEL CALIBRATION

Model	Calibrated input parameters				
	RMS height (cm)	Correlation length (cm)	N* (-)	Litter thickness (cm)	Litter biomass (g/cm^2)
TVG-A	1.2	38.0	1.0	0.9	0.035
TVG-P	0.6	6.0	0.5	0.9	0.035
TVG-AP	2.5	32.0	0.5	0.9	0.035

*N represents the ratio of litter moisture content to soil moisture

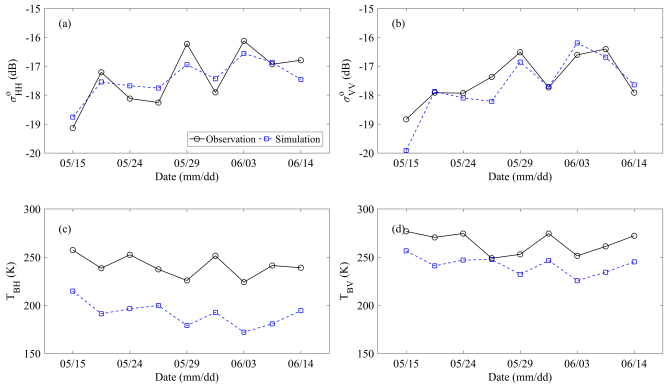

Fig. 7. Temporal evolution of SMAP observations and TVG-A model simulations with calibrated input parameters for (a) σ^o_{HH}, (b) σ^o_{VV}, (c) T_{BH}, and (d) T_{BV}.

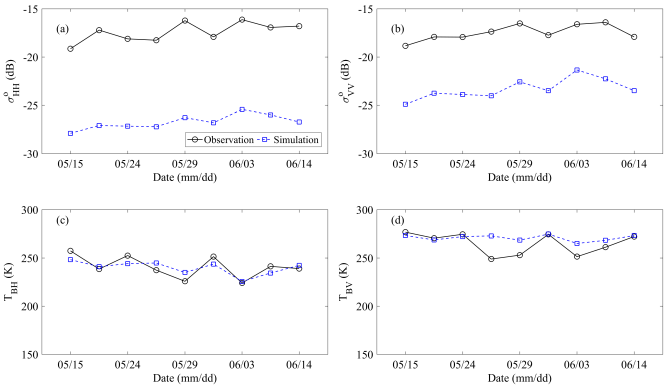

Fig. 8. Temporal evolution of SMAP observations and TVG-P simulations with calibrated input parameters for (a) σ^o_{HH}, (b) σ^o_{VV}, (c) T_{BH}, and (d) T_{BV}.

First, only radar data are applied to calibrate the model, by minimizing the sum of the first two terms of (11), which is considered the TVG-A case. The selected optimal values (see Table II) combined with other previously defined input parameters (see Table I) are used to implement the TVG model in the active and passive configuration simultaneously. Fig. 7 shows the comparisons of SMAP observations and the simulated backscattering coefficients and brightness temperatures obtained from the calibrated TVG-A. It is found that TVG-A is able to simulate the backscattering coefficient well, with R values of 0.91 and 0.90 and RMSE values of 0.48 dB and 0.51 dB for σ^o_{HH} and σ^o_{VV}, respectively. The positive bias indicates that the simulated backscattering coefficient is slightly underestimated.

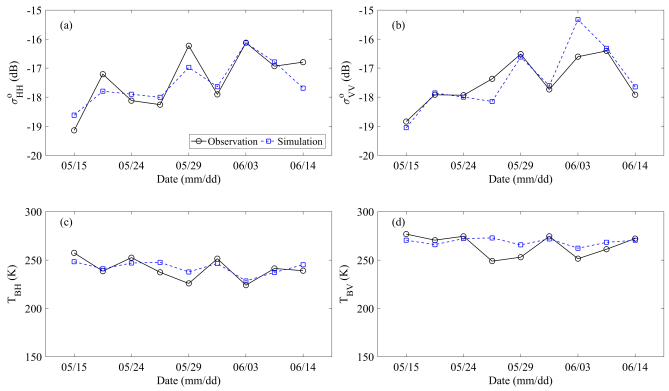

Fig. 9. Temporal evolution of SMAP observations and TVG-AP simulations with calibrated input parameters for (a) σ^o_{HH}, (b) σ^o_{VV}, (c) T_{BH}, and (d) T_{BV}.

TABLE III
ERROR METRICS BETWEEN SMAP OBSERVATIONS AND TVG MODEL SIMULATIONS FOR DIFFERENT POLARIZATIONS DURING MODEL CALIBRATION

Model	Polarization	*R*	*Bias*	*MAE*	*RMSE*	*ubRMSE*
TVG-A	σ^o_{HH} (dB)	0.91	0.03	0.45	0.48	0.48
	σ^o_{VV} (dB)	0.90	0.22	0.38	0.51	0.46
	T_{BH} (K)	0.80	49.57	49.57	50.11	7.33
	T_{BV} (K)	0.65	23.02	23.02	24.46	8.26
TVG-P	σ^o_{HH} (dB)	0.88	9.32	9.32	9.33	0.47
	σ^o_{VV} (dB)	0.88	5.83	5.83	5.85	0.48
	T_{BH} (K)	0.80	0.91	6.24	6.83	6.77
	T_{BV} (K)	0.58	-6.00	7.72	10.96	9.17
TVG-AP	σ^o_{HH} (dB)	0.87	0.09	0.41	0.49	0.48
	σ^o_{VV} (dB)	0.89	-0.07	0.33	0.52	0.51
	T_{BH} (K)	0.78	-1.28	6.55	7.20	7.08
	T_{BV} (K)	0.43	-4.13	8.05	10.47	9.62

Second, only radiometer data are utilized to calibrate the model, by minimizing the last two terms of (11), which is called the TVG-P case. Fig. 8 shows the temporal evolution of the SMAP observations with the simulated backscattering coefficients and brightness temperatures obtained from the calibrated TVG-P. It is observed that the simulation results for brightness temperature are much better than the results obtained from the TVG-A case, as expected. In particular, the values of bias, MAE, and RMSE have conspicuous improvements compared with those of TVG-A. However, T_{BH} is slightly underestimated and T_{BV} is heavily overestimated. The R values between SMAP observations and the TVG-P simulation are 0.80 and 0.58 for T_{BH} and T_{BV}, respectively. In addition, their RMSE values are 6.83 and 10.96 K, respectively, which are slightly high.

In the case of TVG-A, the selected calibrated parameters are prone to good performance for simulating the radar backscatter, and the simulated brightness temperature data deviate significantly from SMAP observations. The same is observed for TVG-P: it can simulate brightness temperature very well but severely underestimates the backscattering coefficient. It is necessary to use both active and passive observations to simultaneously simulate the backscattering coefficient and brightness temperature.

Finally, both radar and radiometer data are used to calibrate the model by minimizing the cost function in (11), which is termed the TVG-AP case. Fig. 9 shows the temporal behavior of the SMAP observations and TVG-AP simulations. In this case, the same input parameters are employed to separately run the model in the active and passive configuration. From the results, it is found that the simulated backscattering coefficients approximate the values obtained from TVG-A and the simulated brightness temperature is close to the results from TVG-P, which demonstrates the effectiveness of the synergistic use of active and passive observations. From the results, it is concluded that the significance of TVG-AP is to find effective values for the model inputs that guarantee the TVG model can simultaneously simulate the backscattering coefficient and brightness temperature very well.

However, it must be noted that the absolute accuracy of brightness temperature (especially T_{BV}) simulated from TVG-P and TVG-AP is relatively lower than that of backscatter simulated from TVG-A and TVG-AP. This phenomenon may be explained by the following two observations. On one hand, the horizontal and vertical mismatch between *in situ* soil moisture and satellite observations will inevitably bring some uncertainties. Many studies have found that compared with radar backscatter, radiometer brightness temperature is more sensitive to soil moisture [4], [63]. Therefore, uncertainties in soil moisture will introduce more deviations in brightness temperature simulations than backscatter simulations. On the other hand, the higher difficulty of modeling emissivity than backscatter may be another explanation for the relatively lower accuracy of brightness temperature simulations. Wave scattering and emission from random rough surfaces are characterized by the bistatic scattering cross section per unit area or surface scattering coefficient. Backscattering is a special case for bistatic scattering in which the transmitter and receiver are colocated [64]. In contrast, the emissivity in a chosen observation direction is equal to one minus reflectivity, expressed as the integral value of the bistatic scattering cross section over the upper half of the space [31], [63]. Numerical accuracy is important to ensure correct results for emissivity in passive remote sensing, as emissivity is related to energy conservation and the accuracy of bistatic scattering coefficients. It is less of a challenge for active monostatic remote sensing as only the backscattering coefficients are calculated on the decibel scale [65]. For instance, Zeng *et al.* [62] conducted a detailed examination of the capability of the AIEM model to predict scattering coefficient and emissivity. They also found that the AIEM model can better simulate backscatter than emissivity (see Tables II and III in their study). This can be a possible explanation for the better accuracy of simulated backscatter relative to that of simulated brightness temperature in our study.

C. Model Validation

Without any further modification, the selected optimal input parameters are used as inputs to the TVG model to simulate the backscattering coefficient and brightness temperature for the

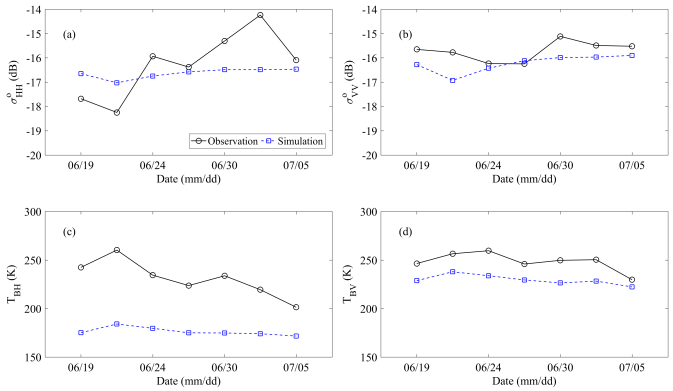

Fig. 10. Temporal evolution of SMAP observations and TVG-A simulations obtained for the validation data for (a) σ^o_{HH}, (b) σ^o_{VV}, (c) T_{BH}, and (d) T_{BV}.

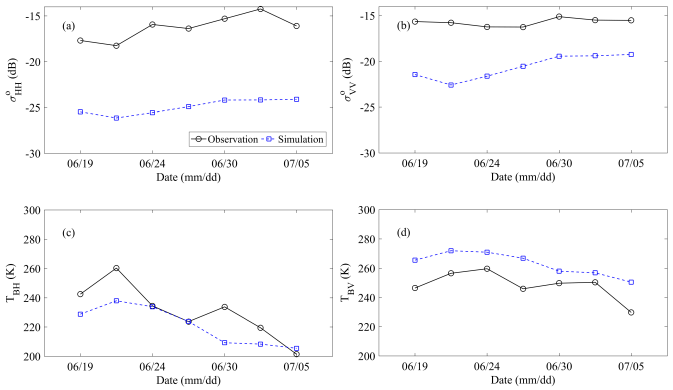

Fig. 11. Temporal evolution of SMAP observations and TVG-P simulations obtained for the validation data for (a) σ^o_{HH}, (b) σ^o_{VV}, (c) T_{BH}, and (d) T_{BV}.

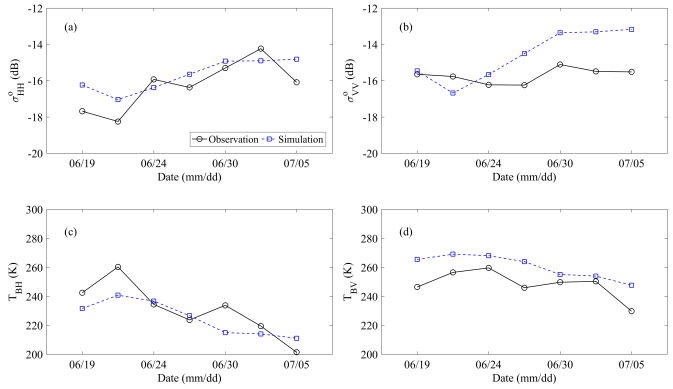

Fig. 12. Temporal evolution of SMAP observations and TVG-AP simulations obtained for the validation data for (a) σ^o_{HH}, (b) σ^o_{VV}, (c) T_{BH}, and (d) T_{BV}.

remaining validation data set. Similar to the procedures used for model calibration, model validation is separately conducted for TVG-A, TVG-P, and TVG-AP. The simulated brightness temperature is obtained by multiplying the simulated emissivity by the *in situ* topsoil temperature. Figs. 10–12 display the temporal evolution of SMAP observations and the simulations from the calibrated TVG model, and their error metrics are given in Table IV.

In general, the model simulations are in good agreement with the SMAP observations, except the brightness temperature simulated from TVG-A and the backscattering coefficient simulated from TVG-P, as expected. In the TVG-AP case, the R between SMAP observations and model simulations are 0.80, 0.55, 0.81, and 0.75, and the RMSE values are 0.96, 1.58 dB, 11.90 K, and 13.53 K for σ^o_{HH}, σ^o_{VV}, T_{BH}, and T_{BV}, respectively. It is found that the simulated σ^o_{HH}, σ^o_{VV}, and T_{BV} values are overestimated and T_{BH} is underestimated.

For TVG-A, the simulated σ^o_{VV} is better than the results of TVG-AP, while the simulated σ^o_{HH} is worse than that of TVG-AP. For TVG-P, the simulated T_{BH} and T_{BV} values are both worse than those of TVG-AP. TVG-AP achieves better results for simulating σ^o_{VV}, T_{BH}, and T_{BV} compared with TVG-A and TVG-P. Nevertheless, the validation results achieved are in slightly worse agreement with SMAP observations compared with the calibration results. The reason may be that the validation period is warmer and has more rain than the calibration period, and the calibration of some input parameters may suffer from these differences.

From the model calibration and validation results, we found two interesting phenomena, which can fully demonstrate the effectiveness of GSA. First, the backscatter simulated from TVG-P is much worse than that from TVG-AP, which confirms the large contribution of rms height and correlation length to simulating the backscattering coefficient; second, the brightness temperature simulated from TVG-A is much worse than that from TVG-AP, which verifies the great importance of litter moisture content for simulating the brightness temperature. These results essentially agree with the results concluded from the calibrated parameters (see Table III). In addition, the results indicate that the sensitive and insensitive parameters for the backscatter coefficient and brightness temperature must be selected carefully through GSA for model calibration.

TABLE IV
ERROR METRICS BETWEEN THE SMAP OBSERVATIONS AND TVG MODEL SIMULATIONS FOR DIFFERENT POLARIZATIONS DURING MODEL VALIDATION

Model	Polarization	*R*	*Bias*	*MAE*	*RMSE*	*ubRMSE*
TVG-A	σ^o_{HH} (dB)	0.74	0.37	1.01	1.19	1.13
	σ^o_{VV} (dB)	0.39	0.51	0.55	0.65	0.39
	T_{BH} (K)	0.85	54.43	54.43	56.22	14.07
	T_{BV} (K)	0.84	18.74	18.74	19.54	5.56
TVG-P	σ^o_{HH} (dB)	0.80	8.68	8.68	8.71	0.79
	σ^o_{VV} (dB)	0.55	4.89	4.89	5.01	1.05
	T_{BH} (K)	0.80	9.74	10.92	14.30	10.47
	T_{BV} (K)	0.78	-14.59	14.59	15.61	5.55
TVG-AP	σ^o_{HH} (dB)	0.80	-0.56	0.88	0.96	0.78
	σ^o_{VV} (dB)	0.55	-1.12	1.38	1.58	1.12
	T_{BH} (K)	0.81	5.68	9.94	11.90	10.45
	T_{BV} (K)	0.75	-12.15	12.15	13.53	5.96

V. DISCUSSION

A. Selection of Sensitive Parameters

In this paper, two parameters (rms height and correlation length) that backscatter is sensitive to and three parameters

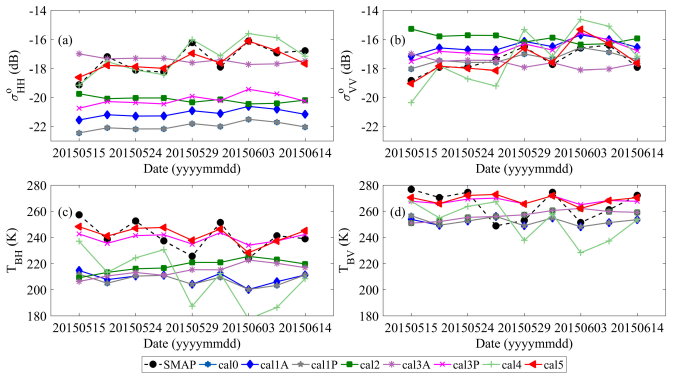

Fig. 13. Temporal evolution of SMAP observations and TVG-AP simulations, with different combinations of sensitive parameters used as free variables for (a) σ^o_{HH}, (b) σ^o_{VV}, (c) T_{BH}, and (d) T_{BV}.

(litter moisture content, litter biomass, and litter thickness) that emissivity is sensitive to are combined as free variables to calibrate the TVG model. The selection of sensitive parameters for use as free variables is very important for model calibration. In the following, comparative experiments are carried out to analyze the influence of several free variables on the calibration accuracy. Taking the TVG-AP model as an example, different combinations of sensitive parameters are used as free variables.

The comparative experiments include the following:

1) no parameters used as free variables, labeled "cal0";
2) only one parameter (rms height) sensitive to backscattering coefficient used as a free variable, labeled "cal1A";
3) only one parameter (litter moisture content) sensitive to emissivity used as a free variable, labeled "cal1P';
4) rms height and litter moisture content combined as free variables, labeled "cal2";
5) rms height, correlation length, and litter moisture content used as free variables, labeled "cal3A";
6) rms height, N, and litter thickness used as free variables, labeled "cal3P";
7) four parameters (rms height, correlation length, litter moisture content, and litter thickness) used as free variables, labeled "cal4";
8) five parameters (rms height, correlation length, litter moisture content, litter biomass, and litter thickness) used as free variables, labeled "cal5."

Fig. 13 presents the temporal evolution of SMAP observations and model simulations with different combinations of sensitive parameters defined as free variables. The calibrated or default values for the five free variables are given in Table V. In all cases, the default values are shown in gray, and the calibrated parameters are shown in bold.

It is clearly observed that the TVG-AP model simulations approach the SMAP observations with an increase of in the number of free variables. The simulated σ^o_{HH} and T_{BH} are generally underestimated, and the bias continuously decreases with the involvement of increased free variables. The simulated σ^o_{VV} fluctuates around the SMAP observations, and the deviation between observed and simulated data is continuously reduced as more free variables are included in the model.

TABLE V

CALIBRATED OR DEFAULT VALUES FOR THE TVG-AP MODEL WITH DIFFERENT COMBINATIONS OF SENSITIVE PARAMETERS USED AS FREE VARIABLES

Case	Calibrated (in bold) or default (in gray) values for the input parameters				
	RMS height (cm)	correlation length (cm)	N* (-)	litter thickness (cm)	litter biomass (g/cm^2)
cal0	0.9	9.0	2.0	0.6	0.07
cal1A	**1.0**	9.0	2.0	0.6	0.07
cal1P	0.9	9.0	**2.0**	0.6	0.07
cal2	**1.2**	9.0	**0.5**	0.6	0.07
cal3A	**1.6**	**36.0**	**0.5**	0.6	0.07
cal3P	**1.4**	9.0	**0.5**	**0.6**	0.07
cal4	**1.6**	**36.0**	**1.0**	**0.6**	0.07
cal5	**2.5**	**32.0**	**0.5**	**0.9**	**0.035**

*N represents the ratio of litter moisture content to soil moisture. Bold text represents the calibrated input parameters, and gray text represents the default values for the input parameters.

The deviations of σ^o_{HH} and T_{BH} are larger than those of σ^o_{VV} and T_{BV}. The TVG-AP simulations achieve the best performance when the five free parameters are used. The dynamics and fluctuations in the TVG-AP model simulations are compromised results between σ^o_{HH} and σ^o_{VV} and T_{BH} and T_{BV} by tuning the values of sensitive parameters. In [30], four parameters, including rms height, litter moisture content, litter biomass, and plant moisture content, are set as free variables using an LSA method to constrain the TVG model. In our study, the plant moisture content is found to be insensitive to backscatter and emissivity, which are defined as empirical values.

Furthermore, it is necessary to assess the contribution of selected sensitive parameters. For the active case, both rms height and correlation length contribute the most to the model simulations. When only the rms height is used, the simulated and observed σ^o_{HH} values have obvious discrepancies. With the addition of correlation length, the accuracy of the simulated σ^o_{HH} is significantly improved. In previous studies, it has often been assumed that the effect of correlation length can be compensated for by rms height [30]. Nevertheless, in our study, we found that the contribution of correlation length cannot be ignored. Comparing the results of "cal1A" and "cal2," it can be observed that the difference between simulated σ^o_{HH} and σ^o_{VV} for these two cases is significant. This demonstrates the weak contribution of litter soil moisture to the radar backscatter. It also indicates that the accuracy of model simulations cannot be significantly improved when insensitive parameters are included. For the passive case, it is also found that the results from three calibrated sensitive parameters are better than the results obtained with one or two calibrated parameters. Comparing the results from "cal3P" and "cal5," it is seen that the simulated brightness temperatures are almost equal. This demonstrates the limited contribution of rms height and correlation length to the brightness temperature, which is consistent with previous studies that have shown that passive observations are less sensitive to surface roughness parameters than are active backscatter observations [4], [10], [11].

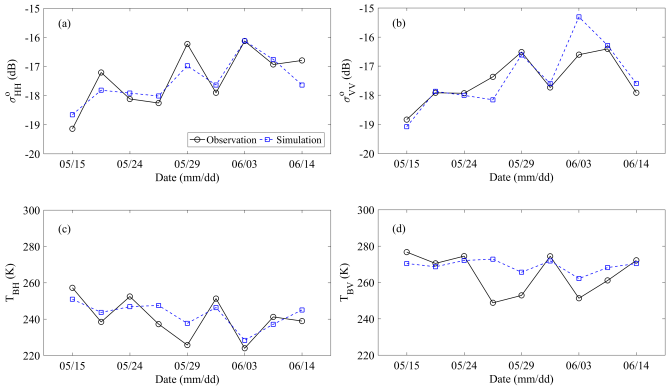

Fig. 14. Temporal evolution of SMAP observations and TVG-AP simulations, with LAI parameterized by their average values for (a) σ^o_{HH}, (b) σ^o_{VV}, (c) T_{BH}, and (d) T_{BV}.

From these results, the principle for the selection of sensitive parameters as free variables can be concluded from two considerations. On one hand, a certain number of sensitive parameters are needed to balance the calibration accuracy and computation. On the other hand, the parameters that are sensitive to the backscattering coefficient and those that are sensitive to the brightness temperature must be combined for TVG-AP model calibration.

B. Contribution of LAI

In previous studies, it has been found that vegetation (mainly represented by VWC or vegetation optical depth) has a substantial influence on backscattering coefficient and brightness temperature [7], [8], [42], [66]. LAI is often assumed to be a good proxy to characterize the attenuation and scattering of vegetation. In this paper, the LAI required by the TVG model is parameterized by the interpolated LAI from MODIS LAI products. However, LAI is selected as a parameter insensitive to the backscatter and emissivity from the results of GSA (see Fig. 6). Thus, in this section, the contribution of LAI in simulating the backscattering coefficient and brightness temperature is analyzed by assuming it to have the average value (0.61 m^2/m^2), which aims to test whether LAI truly affects the final calibration results. Taking the TVG-AP model as an example, the calibration procedures described in Section IV-B. are conducted again with LAI, which is assumed to have a constant value.

When the LAI data required by the TVG-AP model were parameterized by their average values, the optimal values of the five most sensitive parameters for TVG-AP are the same as the values listed in Table II. The rms height, correlation length, N, litter thickness, and litter biomass are 2.5 cm, 32 cm, 0.5, 0.9 cm, and 0.035 g/cm^2, respectively. In this case, the error metrics between the SMAP observations and model simulations shown in Table VI are almost the same as the results displayed in Table III. Fig. 14 shows the temporal evolution of SMAP observations and model simulations with LAI parameterized by their average value. It is observed that the parameterization of LAI has little impact on the simulation of backscattering and emissivity. Accordingly, the LAIs required by the TVG model can be initialized by their average values. From the results of GSA, LAI is insensitive to backscatter and emissivity, and thus can be set as constant. These results further demonstrate the necessity and effectiveness of the application of GSA to model calibration.

TABLE VI
ERROR METRICS BETWEEN SMAP OBSERVATIONS AND TVG-AP MODEL SIMULATIONS WITH LAI PARAMETERIZED BY THEIR AVERAGE VALUES

Model	Polarization	*R*	*Bias*	*MAE*	*RMSE*	*ubRMSE*
TVG-AP	σ^o_{HH} (dB)	0.87	0.09	0.40	0.48	0.47
	σ^o_{VV} (dB)	0.89	-0.08	0.35	0.53	0.52
	T_{BH} (K)	0.80	-1.90	6.55	7.03	6.77
	T_{BV} (K)	0.51	-4.44	7.74	10.37	9.37

C. Uncertainties in Model Calibration

The main purpose of this paper is to explore the feasibility and effectiveness of the synergy of active and passive observations through the unified TVG model, which is achieved by selecting a set of input parameters to parameterize the model for simultaneously simulating the backscattering coefficient and brightness temperature. From previous results and discussion, it is learned that the correctness of model calibration plays an important role in simulating SMAP observations. Therefore, it is necessary to indicate sources of uncertainty that may reduce the accuracy of model calibration. In this paper, uncertainties may come from three aspects: uncertainty from satellite observations, uncertainty from *in situ* measurements, and uncertainty from the limited number of samples.

In this paper, active and passive data at 9 km from the SMAP Level-3 radar/radiometer soil moisture product are used as real satellite observations. The 9 km brightness temperature data in this product are disaggregated from original 36-km radiometer data by using concurrent high resolution radar data. This means the disaggregated brightness temperature is inherently a function of radar backscatter. These data sets may contain artifacts, which will affect the calibration results.

Furthermore, *in situ* measurements were used as soil moisture input in the TVG model to simulate the SMAP backscattering coefficient and brightness temperature. The most challenging issue in such a case is the representativeness of *in situ* measurements in a SMAP pixel. Many studies have shown that using the spatial average of dense *in situ* measurements can reduce the uncertainty resulting from scale-related issues [1], [14], [24], [67], [68]. Therefore, to relieve the spatial resolution inconformity between the SMAP grid and *in situ* location, ground soil moisture measurements from three stations are used and averaged to represent the soil moisture within the SMAP grid. It should be noted that though ground measurements from dense stations are used to minimize the effect of scale-related issues, the differences in spatial resolution will still introduce some deviation [24]. Moreover, the vertical mismatch between the *in situ* soil moisture measuring depth and the microwave penetration depth (commonly, the effective soil moisture sampling depth

at L-band is 0–3 cm and depends on soil moisture) may also contribute to the deviations of the SMAP simulations.

We also calculated the correlation coefficient (R) between *in situ* averaged soil moisture and SMAP radar and radiometer observations. It is found that the *in situ* soil moisture correlates very well with both SMAP active and passive observations. A positive relationship (averaged value of 0.86 for two polarizations) for radar and a negative relationship (averaged value of -0.77) for radiometer are found, as expected. The slightly higher correlation of soil moisture with radar than with radiometer in Maqu network region is consistent with Zeng *et al.* [24], in which they found that the active ASCAT soil moisture product has the highest R value than other passive soil moisture products (e.g., SMOS, AMSR2, and AMSR-E) in the Maqu network region.

We also added additive white Gaussian noise in the *in situ* soil moisture, and perform the same numerical simulation to investigate the effects of input soil moisture uncertainty on the calibrated parameters. We found that the *in situ* soil moisture with small to moderate perturbation (i.e., 2% and 5% perturbation in our simulation) has very small influence on the calibrated parameters. Therefore, we believe our results will not be changed even if there are some (not large) uncertainties in the *in situ* averaged soil moisture.

Moreover, in order to include both calibration and validation procedure, approximately 60% of the data are used to calibrate the model, and the remaining data are used to validate the calibrated parameters. Meanwhile, the leave-one-out cross calibration approach was also performed, and the results are consistent with our current 60/40 split strategy. This supports the reasonableness of our calibration/validation data allocation. Therefore, though some uncertainties may be introduced in the calibrated parameters due to the limited SMAP data, the uncertainties is believed to be small and can be ignored reasonably.

D. Considerations for GSA

Though GSA is capable of distinguishing sensitive and insensitive parameters, which is very helpful for model calibration, some attention is required when applying the EFAST method. On one hand, the ranges of the model parameters play an important role in the SI and the ranking of sensitive parameters. Ma *et al.* [33] analyzed the results of sensitivity analysis associated with various parameter ranges and found that the TSI and MSI depend on the selected ranges of input parameters. Wang *et al.* [61] determined that the range of parameter variation was one of the main factors influencing sensitivity results. For sensor configuration, different frequencies and incidence angles will lead to different scattering and emission mechanisms between the microwave signal and land surface. Therefore, the GSA results conducted in this paper are constrained in the SMAP configuration with defined distributions and variation ranges in the input parameters.

On the other hand, the sample size plays an important role in the convergence of the SI. Previous studies have determined that the SI quickly converges for insensitive parameters and a relatively large sample size is needed to obtain convergence for sensitive parameters [61]. However, a large sample size will increase the amount of computation required and thus decrease the computation efficiency. Therefore, a reasonable sample size must be found to balance convergence and computation. In this paper, we find that the SI converge when the sample size is set to 20 500. To guarantee the stability and reliability of the SI, we set the sample size C as 41 000 during the GSA.

VI. Conclusion

Understanding the scattering and emission mechanisms over the land surface is important for microwave remote sensing modeling and surface parameter retrieval. In this paper, the TVG model is explored to simulate the backscattering coefficient and brightness temperature of SMAP by integrating GSA for the determination of the sensitive and insensitive parameters. This model is driven by a set of input parameters. It is very difficult and time consuming to calibrate the model when all the input parameters are defined as free variables. Thus, the EFAST algorithm, which is recognized as one of the most elegant methods for GSA, is conducted to select the sensitive and insensitive parameters. Only the most sensitive parameters are set as free variables, and they are used to calibrate the model, while the insensitive parameters are set as empirical values. To highlight the advantages of the simultaneous use of active and passive data, available limited-duration and concurrent SMAP radar and radiometer observations are adopted to calibrate and validate the model with three models, including TVG-A, TVG-P, and TVG-AP.

Model calibration is performed using *in situ* and satellite data from May 2015 to early June 2015 by varying the free variables in the defined ranges until the best match between SMAP observations and model simulations is reached. The results show that TVG-AP can find realistic values for the input parameters. This model achieves good agreement between the SMAP observations and model simulations, with R values of 0.87, 0.89, 0.78, and 0.43 and RMSE values of 0.49 dB, 0.52 dB, 7.20 K, and 10.47 K for σ^o_{HH}, σ^o_{VV}, T_{BH}, and T_{BV}, respectively. TVG-A only has good performance in simulating the backscattering coefficient, and TVG-P only achieves reliable results in modeling the brightness temperature. The reasons for these discrepancies are that the calibrated parameters in TVG-A and TVG-P are not optimal when only active or passive data are used. Without any modifications of the calibrated parameters, the backscattering coefficient and brightness temperature simulated by TVG-AP are in slightly worse agreement with SMAP observations for later June 2015 and early July 2015.

In our study, we found that the TVG model can simultaneously simulate the backscattering coefficient and brightness temperature accurately when both SMAP active and passive data are adopted. It can be clearly seen that the TVG model can only predict either backscatter or brightness temperature well when active-only or passive-only observations are used. The results of these simulations, therefore, demonstrate the feasibility and effectiveness of the synergistic use of active–passive observations for model calibration. With a well-calibrated model, we can then analyze the relationship between the backscatter and emissivity and retrieve soil moisture data

from active and passive observations, as well as gain insights into the microwave scattering and emission mechanisms over the land surface. For example, Akbar and Moghaddam [11] and Akbar *et al.* [19], [69] conducted excellent work to develop combined active–passive methodologies based on active–passive forward models to retrieve soil moisture and highlighted the importance and advantage of the synergistic use of active and passive observations to retrieve soil moisture. Zeng *et al.* [70] also adopted a data-driven approach to investigate the covariability of SMAP active–passive observations and its dependence on vegetation and surface roughness. We can further explore this active–passive complementarity, as well as develop an active–passive combined soil moisture algorithm, with a unified and well-calibrated model.

The findings in this paper demonstrate the advantages of the synergistic use of SMAP radar and radiometer data in improving the accuracy of model simulations. In addition, GSA is necessary for selecting the most sensitive parameters for model calibration and simplification. The transferability of the proposed methodology will be tested and validated in more climatically variable and vegetated areas in the future.

ACKNOWLEDGMENT

The authors would like to thank the anonymous reviewers for their helpful comments and suggestions. They would also like to thank the Jet Propulsion Laboratory and NSIDC for making the SMAP data publicly available, and NASA Goddard Space Flight Center and China Meteorological Administration for providing the MODIS data and precipitation data, respectively.

REFERENCES

[1] Z. Su *et al.*, "The Tibetan Plateau observatory of plateau scale soil moisture and soil temperature (Tibet-Obs) for quantifying uncertainties in coarse resolution satellite and model products," *Hydrol. Earth Syst. Sci.*, vol. 15, no. 7, pp. 2303–2316, 2011.

[2] K. C. Kornelsen and P. Coulibaly, "Advances in soil moisture retrieval from synthetic aperture radar and hydrological applications," *J. Hydrol.*, vol. 476, pp. 460–489, Jan. 2013.

[3] G. P. Petropoulos, G. Ireland, and B. Barrett, "Surface soil moisture retrievals from remote sensing: Current status, products & future trends," *Phys. Chem. Earth, A–C*, vols. 83–84, pp. 36–56, Mar. 2015.

[4] Q. Chen *et al.*, "Soil moisture retrieval from SMAP: A validation and error analysis study using ground-based observations over the Little Washita Watershed," *IEEE Trans. Geosci. Remote Sens.*, vol. 56, no. 3, pp. 1394–1408, Mar. 2018.

[5] L. Karthikeyan, M. Pan, N. Wanders, D. N. Kumar, and E. F. Wood, "Four decades of microwave satellite soil moisture observations: Part 1. A review of retrieval algorithms," *Adv. Water Resour.*, vol. 109, pp. 106–120, Nov. 2017.

[6] B. P. Mohanty, M. H. Cosh, V. Lakshmi, and C. Montzka, "Soil moisture remote sensing: State-of-the-science," *Vadose Zone J.*, vol. 16, no. 1, Jan. 2017.

[7] X. Bai *et al.*, "First assessment of Sentinel-1A data for surface soil moisture estimations using a coupled water cloud model and advanced integral equation model over the Tibetan Plateau," *Remote Sens.*, vol. 9, no. 7, p. 714, 2017.

[8] X. Bai, B. He, and X. Li, "Optimum surface roughness to parameterize advanced integral equation model for soil moisture retrieval in prairie area using Radarsat-2 data," *IEEE Trans. Geosci. Remote Sens.*, vol. 54, no. 4, pp. 2437–2449, Apr. 2016.

[9] J. P. Wigneron *et al.*, "Modelling the passive microwave signature from land surfaces: A review of recent results and application to the L-band SMOS & SMAP soil moisture retrieval algorithms," *Remote Sens. Environ.*, vol. 192, pp. 238–262, Apr. 2017.

[10] D. Entekhabi *et al.*, "The Soil Moisture Active Passive (SMAP) mission," *Proc. IEEE*, vol. 98, no. 5, pp. 704–716, May 2010.

[11] R. Akbar and M. Moghaddam, "A combined active–passive soil moisture estimation algorithm with adaptive regularization in support of SMAP," *IEEE Trans. Geosci. Remote Sens.*, vol. 53, no. 6, pp. 3312–3324, Jun. 2015.

[12] D. M. Le Vine, G. S. E. Lagerloef, and S. E. Torrusio, "Aquarius and remote sensing of sea surface salinity from space," *Proc. IEEE*, vol. 98, no. 5, pp. 688–703, May 2010.

[13] R. Bindlish, T. Jackson, M. Cosh, T. Zhao, and P. O'Neill, "Global soil moisture from the aquarius/SAC-D satellite: Description and initial assessment," *IEEE Geosci. Remote Sens. Lett.*, vol. 12, no. 5, pp. 923–927, May 2015.

[14] J. Y. Zeng, K.-S. Chen, H. Bi, and Q. Chen, "A preliminary evaluation of the SMAP radiometer soil moisture product over United States and Europe using ground-based measurements," *IEEE Trans. Geosci. Remote Sens.*, vol. 54, no. 8, pp. 4929–4940, Aug. 2016.

[15] A. Colliander *et al.*, "Validation of SMAP surface soil moisture products with core validation sites," *Remote Sens. Environ.*, vol. 191, pp. 215–231, Mar. 2017.

[16] C. Rüdiger, C.-H. Su, D. Ryu, and W. Wagner, "Disaggregation of low-resolution L-band radiometry using C-band radar data," *IEEE Geosci. Remote Sens. Lett.*, vol. 13, no. 10, pp. 1425–1429, Oct. 2016.

[17] N. N. Das *et al.*, "High-resolution enhanced product based on SMAP active-passive approach using Sentinel 1 data and its applications," in *Proc. IEEE Int. Geosci. Remote Sens. Symp. (IGARSS)*, Jul. 2017, pp. 2543–2545.

[18] J. Shi *et al.*, "WCOM: The science scenario and objectives of a global water cycle observation mission," in *Proc. IEEE Int. Geosci. Remote Sens. Symp. (IGARSS)*, Jul. 2014, pp. 3646–3649.

[19] R. Akbar, M. H. Cosh, P. E. O'Neill, D. Entekhabi, and M. Moghaddam, "Combined radar–radiometer surface soil moisture and roughness estimation," *IEEE Trans. Geosci. Remote Sens.*, vol. 55, no. 7, pp. 4098–4110, Jul. 2017.

[20] R. van der Velde, M. S. Salama, O. A. Eweys, J. Wen, and Q. Wang, "Soil moisture mapping using combined active/passive microwave observations over the east of the Netherlands," *IEEE J. Sel. Topics Appl. Earth Observ. Remote Sens.*, vol. 8, no. 9, pp. 4355–4372, Sep. 2015.

[21] N. N. Das, D. Entekhabi, and E. G. Njoku, "An algorithm for merging SMAP radiometer and radar data for high-resolution soil-moisture retrieval," *IEEE Trans. Geosci. Remote Sens.*, vol. 49, no. 5, pp. 1504–1512, May 2011.

[22] N. N. Das, D. Entekhabi, E. G. Njoku, J. J. C. Shi, J. T. Johnson, and A. Colliander, "Tests of the SMAP combined radar and radiometer algorithm using airborne field campaign observations and simulated data," *IEEE Trans. Geosci. Remote Sens.*, vol. 52, no. 4, pp. 2018–2028, Apr. 2014.

[23] Y. Y. Liu *et al.*, "Trend-preserving blending of passive and active microwave soil moisture retrievals," *Remote Sens. Environ.*, vol. 123, pp. 280–297, Aug. 2012.

[24] J. Zeng, Z. Li, Q. Chen, H. Bi, J. Qiu, and P. Zou, "Evaluation of remotely sensed and reanalysis soil moisture products over the Tibetan Plateau using *in-situ* observations," *Remote Sens. Environ.*, vol. 163, pp. 91–110, Jun. 2015.

[25] J. Kolassa, P. Gentine, C. Prigent, and F. Aires, "Soil moisture retrieval from AMSR-E and ASCAT microwave observation synergy. Part 1: Satellite data analysis," *Remote Sens. Environ.*, vol. 173, pp. 1–14, Feb. 2016.

[26] J. Kolassa, P. Gentine, C. Prigent, F. Aires, and S. H. Alemohammad, "Soil moisture retrieval from AMSR-E and ASCAT microwave observation synergy. Part 2: Product evaluation," *Remote Sens. Environ.*, vol. 195, pp. 202–217, Jun. 2017.

[27] E. Santi, S. Paloscia, S. Pettinato, and G. Fontanelli, "Application of artificial neural networks for the soil moisture retrieval from active and passive microwave spaceborne sensors," *Int. J. Appl. Earth Observ. Geoinf.*, vol. 48, pp. 61–73, Jun. 2016.

[28] M. Barber, C. Bruscantini, F. Grings, and H. Karszenbaum, "Bayesian combined active/passive (B-CAP) soil moisture retrieval algorithm," *IEEE J. Sel. Topics Appl. Earth Observ. Remote Sens.*, vol. 9, no. 12, pp. 5449–5460, Dec. 2016.

[29] L. Dente, P. Ferrazzoli, Z. Su, R. van de Velde, and L. Guerriero, "Combined use of active and passive microwave satellite data to constrain a discrete scattering model," *Remote Sens. Environ.*, vol. 155, pp. 222–238, Dec. 2014.

[30] Q. Wang, R. van der Velde, and Z. Su, "Use of a discrete electromagnetic model for simulating Aquarius L-band active/passive observations and soil moisture retrieval," *Remote Sens. Environ.*, vol. 205, pp. 434–452, Feb. 2017.

[31] M. Piles, K. A. McColl, D. Entekhabi, N. Das, and M. Pablos, "Sensitivity of Aquarius active and passive measurements temporal covariability to land surface characteristics," *IEEE Trans. Geosci. Remote Sens.*, vol. 53, no. 8, pp. 4700–4711, Aug. 2015.

[32] K. A. McColl, D. Entekhabi, and M. Piles, "Uncertainty analysis of soil moisture and vegetation indices using Aquarius scatterometer observations," *IEEE Trans. Geosci. Remote Sens.*, vol. 52, no. 7, pp. 4259–4272, Jul. 2014.

[33] C. Ma, X. Li, and S. Wang, "A global sensitivity analysis of soil parameters associated with backscattering using the advanced integral equation model," *IEEE Trans. Geosci. Remote Sens.*, vol. 53, no. 10, pp. 5613–5623, Oct. 2015.

[34] A. Saltelli and P. Annoni, "How to avoid a perfunctory sensitivity analysis," *Environ. Model. Softw.*, vol. 25, no. 12, pp. 1508–1517, 2010.

[35] Y. Gan *et al.*, "A comprehensive evaluation of various sensitivity analysis methods: A case study with a hydrological model," *Environ. Model. Softw.*, vol. 51, pp. 269–285, Jan. 2014.

[36] M. Bracaglia, P. Ferrazzoli, and L. Guerriero, "A fully polarimetric multiple scattering model for crops," *Remote Sens. Environ.*, vol. 54, no. 3, pp. 170–179, 1995.

[37] P. Ferrazzoli and L. Guerriero, "Passive microwave remote sensing of forests: A model investigation," *IEEE Trans. Geosci. Remote Sens.*, vol. 34, no. 2, pp. 433–443, Mar. 1996.

[38] V. Barraza *et al.*, "Monitoring vegetation moisture using passive microwave and optical indices in the Dry Chaco Forest, Argentina," *IEEE J. Sel. Topics Appl. Earth Observ. Remote Sens.*, vol. 7, no. 2, pp. 421–430, Feb. 2014.

[39] D. Zheng *et al.*, "L-band microwave emission of soil freeze–thaw process in the third pole environment," *IEEE Trans. Geosci. Remote Sens.*, vol. 55, no. 9, pp. 5324–5338, Sep. 2017.

[40] A. Saltelli, S. Tarantola, and K. P.-S. Chan, "A quantitative model-independent method for global sensitivity analysis of model output," *Technometrics*, vol. 41, no. 1, pp. 39–56, 1999.

[41] L. Dente, Z. Vekerdy, J. Wen, and Z. Su, "Maqu network for validation of satellite-derived soil moisture products," *Int. J. Appl. Earth Observ. Geoinf.*, vol. 17, pp. 55–65, Jul. 2012.

[42] C. Cui *et al.*, "Soil moisture mapping from satellites: An intercomparison of SMAP, SMOS, FY3B, AMSR2, and ESA CCI over two dense network regions at different spatial scales," *Remote Sens.*, vol. 10, no. 1, p. 33, 2018.

[43] A. Savitzky and M. J. E. Golay, "Smoothing and differentiation of data by simplified least squares procedures," *Anal. Chem.*, vol. 36, no. 8, pp. 1627–1639, 1964.

[44] H. J. Eom and A. K. Fung, "Scattering from a random layer embedded with dielectric needles," *Remote Sens. Environ.*, vol. 19, no. 2, pp. 139–149, 1986.

[45] M. A. Karam and A. K. Fung, "Electromagnetic scattering from a layer of finite length, randomly oriented, dielectric, circular cylinders over a rough interface with application to vegetation," *Int. J. Remote Sens.*, vol. 9, no. 6, pp. 1109–1134, 1988.

[46] R. Schiffer and K. O. Thielheim, "Light scattering by dielectric needles and disks," *J. Appl. Phys.*, vol. 50, no. 4, pp. 2476–2483, 1979.

[47] D. M. LeVine, R. Meneghini, R. H. Lang, and S. S. Seker, "Scattering from arbitrarily oriented dielectric disks in the physical optics regime," *J. Opt. Soc. Amer.*, vol. 73, no. 10, pp. 1255–1262, 1983.

[48] A. K. Fung, *Microwave Scattering and Emission Models and Their Applications*. Boston, MA, USA: Artech House, 1994, pp. 62–362.

[49] H. J. Eom and A. K. Fung, "A scatter model for vegetation up to Ku-band," *Remote Sens. Environ.*, vol. 15, no. 3, pp. 185–200, 1984.

[50] C. Mätzler, "Microwave (1–100 GHz) dielectric model of leaves," *IEEE Trans. Geosci. Remote Sens.*, vol. 32, no. 4, pp. 947–949, Jul. 1994.

[51] M. C. Dobson, F. T. Ulaby, M. T. Hallikainen, and M. A. El-Rayes, "Microwave dielectric behavior of wet soil—Part II: Dielectric mixing models," *IEEE Trans. Geosci. Remote Sens.*, vol. GRS-23, no. 1, pp. 35–46, Jan. 1985.

[52] L. Guerriero, P. Ferrazzoli, C. Vittucci, R. Rahmoune, M. Aurizzi, and A. Mattioni, "L-band passive and active signatures of vegetated soil: Simulations with a unified model," *IEEE J. Sel. Topics Appl. Earth Observ. Remote Sens.*, vol. 9, no. 6, pp. 2520–2531, Jun. 2016.

[53] L. Guerriero, N. Pierdicca, L. Pulvirenti, and P. Ferrazzoli, "Use of satellite radar bistatic measurements for crop monitoring: A simulation study on corn fields," *Remote Sens.*, vol. 5, no. 2, pp. 864–890, 2013.

[54] P. Ferrazzoli, J. P. Wigneron, L. Guerriero, and A. Chanzy, "Multifrequency emission of wheat: Modeling and applications," *IEEE Trans. Geosci. Remote Sens.*, vol. 38, no. 6, pp. 2598–2607, Nov. 2000.

[55] A. D. Vecchia, P. Ferrazzoli, J. P. Wigneron, and J. P. Grant, "Modeling forest emissivity at L-band and a comparison with multitemporal measurements," *IEEE Geosci. Remote Sens. Lett.*, vol. 4, no. 4, pp. 508–512, Oct. 2007.

[56] S. Lv, J. Wen, Y. Zeng, H. Tian, and Z. Su, "An improved two-layer algorithm for estimating effective soil temperature in microwave radiometry using *in situ* temperature and soil moisture measurements," *Remote Sens. Environ.*, vol. 152, pp. 356–363, Sep. 2014.

[57] J.-P. Wigneron, A. Chanzy, P. de Rosnay, C. Rudiger, and J.-C. Calvet, "Estimating the effective soil temperature at L-band as a function of soil properties," *IEEE Trans. Geosci. Remote Sens.*, vol. 46, no. 3, pp. 797–807, Mar. 2008.

[58] S. Lv, Y. Zeng, J. Wen, D. Zheng, and Z. Su, "Determination of the optimal mounting depth for calculating effective soil temperature at L-band: Maqu case," *Remote Sens.*, vol. 8, no. 6, p. 476, 2016.

[59] J. P. Grant, J.-P. Wigneron, A. A. Van de Griend, A. Kruszewski, S. S. Søbjærg, and N. Skou, "A field experiment on microwave forest radiometry: L-band signal behaviour for varying conditions of surface wetness," *Remote Sens. Environ.*, vol. 109, no. 1, pp. 10–19, 2007.

[60] M. W. J. Davidson, T. L. Toan, F. Mattia, G. Satalino, T. Manninen, and M. Borgeaud, "On the characterization of agricultural soil roughness for radar remote sensing studies," *IEEE Trans. Geosci. Remote Sens.*, vol. 38, no. 2, pp. 630–640, Mar. 2000.

[61] J. Wang, X. Li, L. Lu, and F. Fang, "Parameter sensitivity analysis of crop growth models based on the extended Fourier amplitude sensitivity test method," *Environ. Model. Softw.*, vol. 48, pp. 171–182, Oct. 2013.

[62] J. Zeng, K.-S. Chen, H. Bi, T. Zhao, and X. Yang, "A comprehensive analysis of rough soil surface scattering and emission predicted by AIEM with comparison to numerical simulations and experimental measurements," *IEEE Trans. Geosci. Remote Sens.*, vol. 55, no. 3, pp. 1696–1708, Mar. 2017.

[63] F. T. Ulaby and D. Long, *Microwave Radar and Radiometric Remote Sensing*. Ann Arbor, MI, USA: Univ. Michigan Press, 2014.

[64] J. Zeng, K.-S. Chen, H. Bi, Q. Chen, and X. Yang, "Radar response of off-specular bistatic scattering to soil moisture and surface roughness at L-band," *IEEE Geosci. Remote Sens. Lett.*, vol. 13, no. 12, pp. 1945–1949, Dec. 2016.

[65] P. Xu and L. Tsang, "Bistatic scattering and emissivities of lossy dielectric surfaces with exponential correlation functions," *IEEE Trans. Geosci. Remote Sens.*, vol. 45, no. 1, pp. 62–72, Jan. 2007.

[66] A. G. Konings, M. Piles, N. Das, and D. Entekhabi, "L-band vegetation optical depth and effective scattering albedo estimation from SMAP," *Remote Sens. Environ.*, vol. 198, pp. 460–470, Sep. 2017.

[67] T. J. Jackson *et al.*, "Validation of advanced microwave scanning radiometer soil moisture products," *IEEE Trans. Geosci. Remote Sens.*, vol. 48, no. 12, pp. 4256–4272, Dec. 2010.

[68] S. K. Chan *et al.*, "Assessment of the SMAP passive soil moisture product," *IEEE Trans. Geosci. Remote Sens.*, vol. 54, no. 8, pp. 4994–5007, Aug. 2016.

[69] R. Akbar, N. Das, D. Entekhabi, and M. Moghaddam, "Active and passive microwave remote sensing synergy for soil moisture estimation," in *Satellite Soil Moisture Retrieval: Techniques and Applications*. Amsterdam, The Netherlands: Elsevier, 2016, pp. 187–207.

[70] J. Zeng *et al.*, "Covariation of SMAP active and passive measurements with respect to vegetation and surface roughness," in *Proc. IEEE IGARSS*, Jul. 2017, pp. 4166–4169.

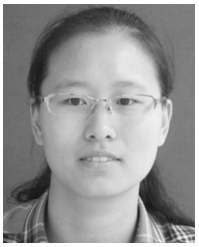

Xiaojing Bai received the B.S. degree in electronic information science and technology from Binzhou University, Binzhou, China, in 2010, and the M.S. and Ph.D. degrees in control engineering and information and communication engineering from the University of Electronic Science and Technology of China, Chengdu, China, in 2013 and 2017, respectively.

She is currently a Lecturer with the School of Hydrology and Water Resources, Nanjing University of Information Science and Technology, Nanjing, China. Her research interests include soil moisture retrieval from active and passive microwave remote sensing.

Jiangyuan Zeng (M'16) received the B.S. degree from Wuhan University, Wuhan, China, in 2010, and the Ph.D. degree from the Institute of Remote Sensing and Digital Earth, Chinese Academy of Sciences, Beijing, China, in 2015.

He is currently an Associate Professor with the State Key Laboratory of Remote Sensing Science, Institute of Remote Sensing and Digital Earth, Chinese Academy of Sciences, Beijing. His research interests include microwave remote sensing of soil moisture, hydrological applications of satellite remote sensing and bistatic scattering of soil surfaces.

Dr. Zeng was a recipient of the Young Scientist Award (including Cash Award) from the Progress in Electromagnetics Research Symposium in 2018, the Young Scientist Award from the International Union of Radio Science in 2017, the Excellent Doctoral Dissertation of the Chinese Academy of Sciences Award in 2016, the Beijing Outstanding Graduates Award, the "ZhuLi YueHua" Excellent Doctoral Student Scholarship of the Chinese Academy of Sciences in 2015, the Chinese Academy of Sciences-BHP Billiton Scholarship Award, and the President Award of the Chinese Academy of Sciences in 2014.

Kun-Shan Chen (S'86–M'92–SM'98–F'07) received the Ph.D. degree in electrical engineering from the University of Texas at Arlington, Arlington, TX, USA, in 1990.

From 1992 to 2014, he was a Faculty Member with National Central University, Taoyuan, Taiwan, where was a Distinguished Chair Professor from 2008 to 2014. He joined the Institute of Remote Sensing and Digital Earth, Chinese Academy of Science, Beijing, China, in 2014, where he is involved in microwave remote sensing theory, modeling, system, and measurement from terrain with applications to environmental watch. He has been a Research Professor with the Department of Electrical Engineering, The University of Texas at Arlington, Arlington, TX, USA, since 2014. He has authored and co-authored over 130 referred journal papers, contributed nine book chapters, co-authored (with A. K. Fung) the *Microwave Scattering and Emission Models for Users*, Artech House, 2010, and authored the *Principles of Synthetic Aperture Radar: A System Simulation Approach*, CRC Press, 2015, and co-edited *Advances in SAR Remote Sensing of Ocean*, CRC Press, 2018.

Dr. Chen was a IEEE GRSS ADCOM Member from 2010 to 2014. He was a Guest Editor for the IEEE TGARS SPECIAL ISSUE ON REMOTE SENSING FOR MAJOR DISASTER PREVENTION, MONITORING AND ASSESSMENT in 2007, the Guest Editor for the PROCEEDINGS OF IEEESPECIAL ISSUE ON REMOTE SENSING FOR NATURAL DISASTER in 2012, a Founding Chair of the GRSS Taipei Chapter, has been an Associate Editor of the IEEE TRANSACTIONS ON GEOSCIENCE AND REMOTE SENSING since 2000, as a founding Deputy Editor-in-Chief of the IEEE JOURNAL OF SELECTED TOPICS IN APPLIED EARTH OBSERVATIONS AND REMOTE SENSING from 2008 to 2010. He serves as a Guest Editor of the special issue of *Data Restoration and Denoising of Remote Sensing Data*, and special issues of *Radar Imaging Theory, Techniques, and Applications*, both for Remote Sensing. He has been a member of the Editorial Board of the Proceedings of the IEEE since 2014.

Zhen Li (M'09) received the B.S. degree in photogrammetry and remote sensing from Wuhan University, Wuhan, China, in 1988, and the Ph.D. degree in natural geography from the Cold and Arid Regions Environmental and Engineering Research Institute, Chinese Academy of Sciences, Lanzhou, China, in 1998.

He is currently a Professor and the Director of the Airborne Remote Sensing Center, Institute of Remote Sensing and Digital Earth, Chinese Academy of Sciences, Beijing, China. He has authored over 80 journal papers and four books in collaboration with others. His research interests include microwave remote sensing with emphasis on remote sensing methods and applications for the land surface, such as microwave modeling and inversion methods of snow, glacier and soil moisture, SAR/InSAR image processing techniques.

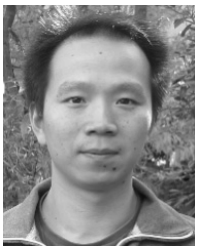

Yijian Zeng received the Ph.D. degree from the University of Twente, Enschede, The Netherlands, in 2012.

He is currently an Assistant Professor with the Faculty of Geo-Information Science and Earth Observation, Water Resources Department, University of Twente. His research interests include land-atmosphere interaction via hydrologic processes and how the interaction affects the climate system, generation of consistent climate data record using multisource of geo-data sets, physical mechanisms of land surface models, and the application of data assimilation.

Jun Wen received the B.A. degree in meteorology from Peking University, Beijing, China, in 1988, the M.A. degree in meteorology from Lanzhou University, Lanzhou, China, in 1995, and the Ph.D. degree in meteorology from the Chinese Academy of Sciences, Lanzhou, in 1999.

He is currently a Professor with the College of Atmospheric Sciences, Chengdu University of Information Technology, Chengdu, China. His research interests include remote sensing and land surface modeling, and climate change.

Xin Wang received the B.A. degree in atmospheric science from Nanjing University, Nanjing, China, in 2007, and the Ph.D. degree in meteorology from University of Chinese Academy of Sciences, China, in 2012.

He is currently an Assistant Professor with the Northwest Institute of Eco-Environment and Resources, Chinese Academy of Sciences, Lanzhou, China. His research interests include soil moisture and freeze/thaw cycle observation, remote sensing and data assimilation, soil moisture retrieval using both active and passive microwave measurement in Tibet, and remote sensing land hydrological cycle in Yellow River source catchment with passive microwave both on ground-based and spaceborne radiometer measurements.

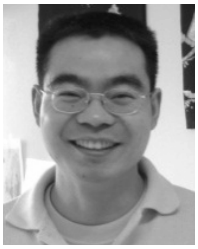

Xiaohua Dong received the B.S. and M.S. degrees from the Hubei University of Technology, Wuhan, China, in 1993 and 1996, and the Ph.D. degree from the University of Twente, Enschede, The Netherlands.

He is currently a Professor with the College of Hydraulic and Environmental Engineering, China Three Gorges University, Yichang, China. His research interests include the investigation of the physics and modeling methods of the hydrological processes, include the infiltration and accompanying processes in soil, evapotranspiration of plants, carbon and phosphorous cycle processes in Karst and phosphate mining areas, hydrologic simulation by using distributed models, hydrologic responses under changing conditions (land use change and climate change).

Zhongbo (Bob) Su received the B.Sc. degree in hydraulic engineering from the Taiyuan University of Technology, Taiyuan, China, the M.Sc. degree in hydrological engineering from the IHE Delft Institute for Water Education, Delft, The Netherlands, and the Ph.D. degree in civil engineering from the Ruhr University, Bochum, Germany.

He is currently a Professor of spatial hydrology and water resources management with the Faculty of Geo-Information Science and Earth Observation, Department of Water Resources, University of Twente, Enschede, The Netherlands. His research interests include remote sensing and numerical modeling of land surface processes and interactions with the atmosphere, earth observation of water cycle and applications in climate, ecosystem and water resources studies, as well as monitoring food security and water-related disasters.

Dr. Su leads the SMAP Core Cal/Val Sites on the Eurasia continent (https://www.itc.nl/wrs/) and serves on the Copernicus L-Band SAR Mission Advisory Group and GEWEX Scientific Steering Group.